Journal of Rock Mechanics and Geotechnical Engineering 14 (2022) 272–288

Contents lists available at ScienceDirect

Journal of Rock Mechanics and Geotechnical Engineering

journal homepage: www.jrmge.cn

Full Length Article

Analysis of ground deformation development and settlement prediction by air-boosted vacuum preloading

Shuangxi Feng [a], Huayang Lei [a,b,c,*], Cheng Lin [d]

[a] Department of Civil Engineering, Tianjin University, Tianjin, 300354, China
[b] Key Laboratory of Coast Civil Structure Safety of the Ministry of Education, Tianjin University, Tianjin, 300354, China
[c] Key Laboratory of Comprehensive Simulation of Engineering Earthquake and Urban-Rural Seismic Resilience, China Earthquak Administration, Tianjin, 300354, China
[d] Department of Civil Engineering, University of Victoria, Victoria, BC, V8P 5C2, Canada

ARTICLE INFO

Article history:
Received 14 January 2021
Received in revised form
31 March 2021
Accepted 9 May 2021
Available online 13 July 2021

Keywords:
Air-boosted vacuum preloading
Field test
Numerical modeling
Settlement
Soft soils
Ground improvement

ABSTRACT

Vacuum preloading has been widely used to improve soft soils in coastal areas of China. An increasing amount of evidence from field operations has shown that conventional vacuum preloading is prone to clogging in prefabricated vertical drains (PVDs) and demands a large volume of sand fills. In recent years, air-boosted vacuum preloading has been developed to overcome these limitations; however, this method still requires more data to verify its performance. In this study, a field test for air-boosted vacuum preloading was conducted, and a large-strain two-dimensional (2D) finite element (FE) model was developed and validated against the field test data. Then, a series of FE parametric analyses was performed to assess key factors, i.e. the air injection pressure, the injection spacing, and the characteristics of cyclic injection, which affect the performance of the air-boosted vacuum preloading. The results showed that the ground settlement and lateral displacement of the soils increased due to an increase in the injection pressure, a decrease in the injection spacing, or increases in the number and duration of the injection cycles. Based on the parametric analyses, an empirical formula for ground settlement prediction was proposed and compared with a case history reported in the literature, showing good agreement.

1. Introduction

The rapid economic growth in coastal areas of China calls for the development of more space to sustain the growth; however, for the coastal cities with dense populations and a shortage of land, this appears to be a great challenge. Land reclamation has been considered as an effective solution to grapple with this issue as it creates new land from the adjacent water through depositing the dredged sediments. The reclaimed ground is too weak to hold buildings, ports, or other infrastructure systems. Therefore, ground improvement techniques are typically implemented to strengthen the deposits; among these techniques, vacuum preloading is widely utilized to treat soft ground due to its low unit cost and high construction efficiency. Vacuum preloading is the process of applying a negative or vacuum pressure in the ground, thereby creating a pressure gradient between drainage channels (usually prefabricated vertical drains (PVDs)) and surrounding soils. The negative pressure continuously draws pore water out of the ground, which, therefore, can speed up consolidation of the soils (Indraratna et al., 2019; Gouw, 2020). This method was first proposed by Kjellman (1952) to improve the consolidation of soil deposits at the Philadelphia International Airport, USA. Currently, it is a standard method for treating soft dredged deposits in the coastal cities of Asia. However, with its increasing application, the vacuum preloading method has shown some drawbacks in sustaining desirable performance, especially in regard to the treatment of reclaimed ground (Shen et al., 2015; Gangaputhiran et al., 2016). For example, PVDs are susceptible to bending and clogging as a result of incompatible stiffness between the soils and the PVDs, which reduces the vacuum pressures in both the sand blanket and the PVDs, thereby undermining the efficiency of vacuum preloading (Lei et al., 2017). Moreover, owing to the stringent environmental protection policies in the coastal areas of China, the demand for sands for the construction of the sand blanket has increased substantially,

* Corresponding author. Department of Civil Engineering, Tianjin University, Tianjin, 300354, China.
E-mail address: leihuayang74@163.com (H. Lei).
Peer review under responsibility of Institute of Rock and Soil Mechanics, Chinese Academy of Sciences.

https://doi.org/10.1016/j.jrmge.2021.05.006

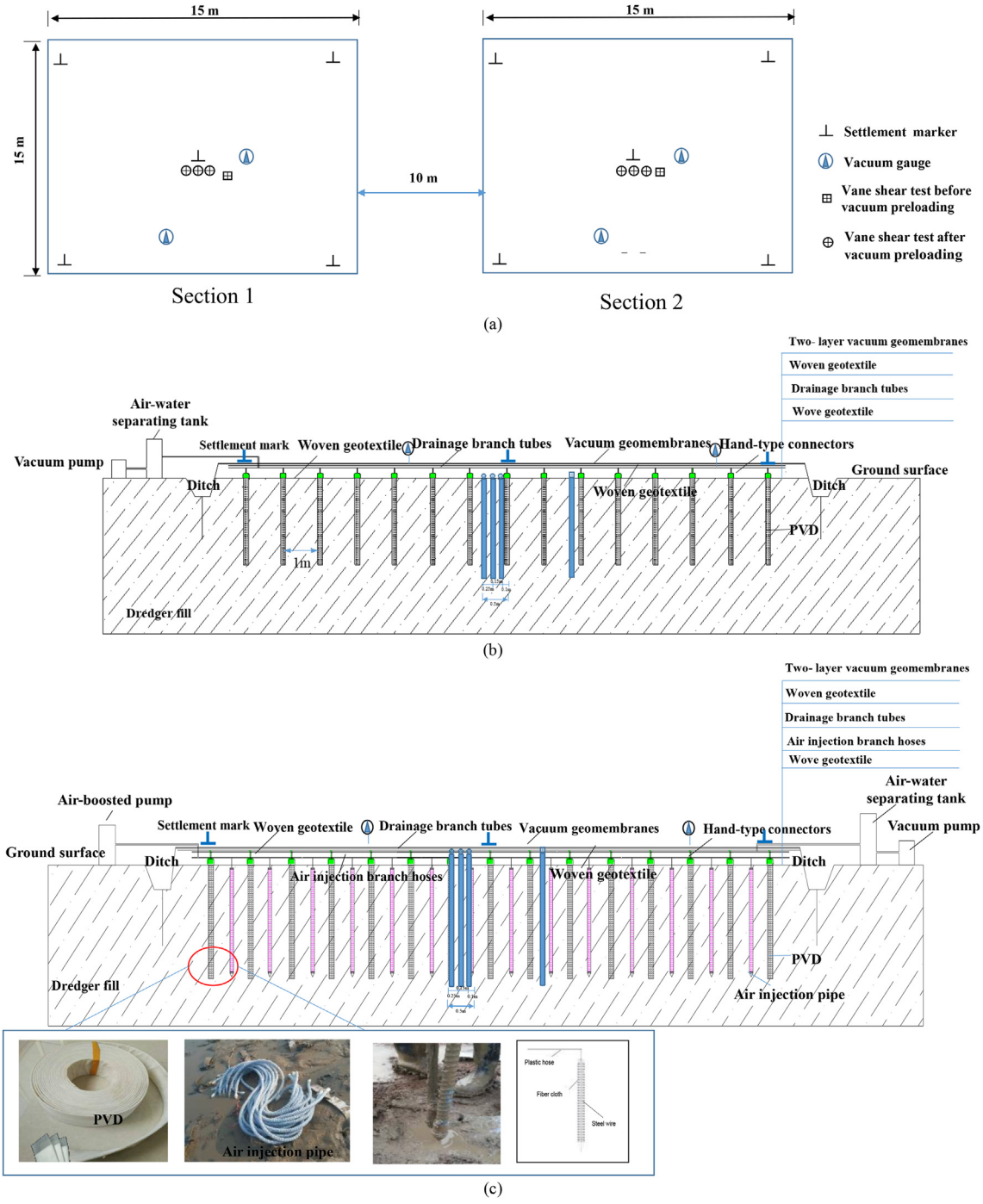

Fig. 1. Plan and cross-sectional views of the test site and instrumentation: (a) Planar graph for conventional and air-boosted vacuum preloading; (b) Sectional drawing for conventional vacuum preloading; and (c) Sectional drawing for air-boosted vacuum preloading.

resulting in a significant surge of construction cost (Mesri and Khan, 2012; Liu et al., 2017a).

To overcome these limitations, an innovative method, called air-boosted vacuum preloading, has been developed in recent years (Nguyen et al., 2018). This method adds an air-boosted system to the vacuum preloading system. The air-boosted system consists of air injection pipes, booster pumps, and plastic hoses, while the vacuum preloading system is upgraded from the conventional vacuum preloading system by replacing the costly sand blanket with a wire hose as the horizontal drainage system. A salient feature of air-boosted vacuum preloading is that it creates an extra pressure gradient between the soft soil and the PVDs through the addition of air injection pipes. This additional pressure helps to further accelerate soil consolidation, and thus improves the treatment efficiency.

Numerous studies have employed numerical simulations and field tests to evaluate the performance of air-boosted vacuum preloading and its underlying mechanisms. Voottipruex et al.

(2013) used numerical models to assess the performance of air-boosted vacuum preloading for the improvement of weak ground. They found that the treatment effectiveness was improved as the injected air pressure increased. Based on a full-scale field test, Wang et al. (2016) reported that the degree of consolidation was improved by the air-boosted vacuum preloading (i.e. 85.7%) compared with the conventional vacuum preloading (i.e. 70.1%) on the 108th day. Cai et al. (2018) also evaluated the air-boosted vacuum preloading for deep marine clays based on field tests and confirmed the benefits of the air-boosted vacuum preloading in accelerating ground settlement.

Although past studies have demonstrated the benefits of air-boosted vacuum preloading, several key factors influencing its performance for mass treatment of soft soil ground are still not understood. These key factors include the air injection pressure, the injection spacing, and the injection cycles and durations. The objective of this study was to document a full-scale field test program comparing the air-boosted vacuum preloading method with the conventional vacuum preloading method. A two-dimensional (2D) continuum finite element (FE) model was then established and validated against the field test data. The 2D FE model was further used to conduct the parametric analyses to evaluate the effects of these key factors on the performance of the air-boosted vacuum preloading. The FE results, including ground settlement and lateral displacement of soils, were discussed, with an emphasis on their implications for the design and construction of an air-boosted vacuum preloading system. Finally, based on the numerical analysis results, an empirical equation was developed to predict the ground settlement, which is capable of considering various injection pressures, injection spacings, and injection cycles and durations.

2. Field test program

Field tests of both conventional and air-boosted vacuum preloading were conducted at a reclaimed land site (approximately 98,000 m^2 in area) in the Lingang Area of Tianjin, China. As shown in Fig. 1, two test sections, each measuring 15 m × 15 m, were treated with the conventional vacuum preloading (S1) and the air-boosted vacuum preloading (S2), respectively. The ground elevation was surveyed before and after the vacuum preloading, where the datum was the mean sea level of the Yellow Sea in China. According to the survey, the initial ground surface was at an elevation of +5.5 m. The field test program included subsurface soil investigation, test site construction, and settlement monitoring. The details of the field tests are presented in the following sections.

2.1. Subsurface soil conditions

Subsurface soil conditions were explored by drilling four boreholes to a depth of 16.9 m below the ground surface. The generalized soil profile is given in Table 1. In general, the subsurface soils within the explored depth were fat clay overlying lean clay. The lean clay was further divided into three layers because of their considerably different soil properties. In each layer, soil samples were obtained for a series of laboratory tests, including basic index tests, consolidated-drained (CD) triaxial tests, and falling-head permeability tests. These tests were performed in accordance with the Chinese standard for soil testing (GB/T 50123–2019, 2019). Both horizontal and vertical hydraulic conductivities were measured by testing smaller samples (ϕ61.8 mm × 40 mm) that were cut out of the horizontal and vertical surfaces of the Shelby tube samples (ϕ100 mm × 500 mm), respectively, as shown in Fig. 2.

The laboratory test results are summarized in Table 1. The water content was in excess of the liquid limit, which in general indicated a normally consolidated or unconsolidated soil. The initial void ratio was high, all exceeding 1. The hydraulic conductivity was on the order of 10^{-7} cm/s to 10^{-6} cm/s, which falls in the typical range for clay. In Table 1, the coefficient of the at-rest earth pressure was calculated using Jaky's equation ($k_0 = 1 - \sin\varphi'$, where φ' is the effective internal friction angle) by assuming that the soils were normally consolidated.

Table 1
Soil properties.

Parameter	Fat clay	Lean clay 1	Lean clay 2	Lean clay 3
Thickness (m)	2.6	3.1	6.2	5
Water content (%)	66.5	54.3	55.1	45.1
Density (g/cm^3)	1.84	1.87	1.92	1.87
Liquid limit (%)	55	43	38	31
Plastic limit (%)	30	25	21	15
Initial void ratio	1.22	1.21	1.12	1.07
Cohesion (kPa)	4.2	3.8	18.3	14.4
Internal friction angle (°)	6	5	4	7
Poisson's ratio	0.35	0.32	0.3	0.32
Coefficient of earth pressure	0.89	0.91	0.93	0.88
Horizontal hydraulic conductivity (m/d)	0.00078	0.00069	0.0087	0.0076
Vertical hydraulic conductivity (m/d)	0.00078	0.00067	0.0069	0.0058
Drained elastic modulus (MPa)	2.5	2.8	2.6	2.8

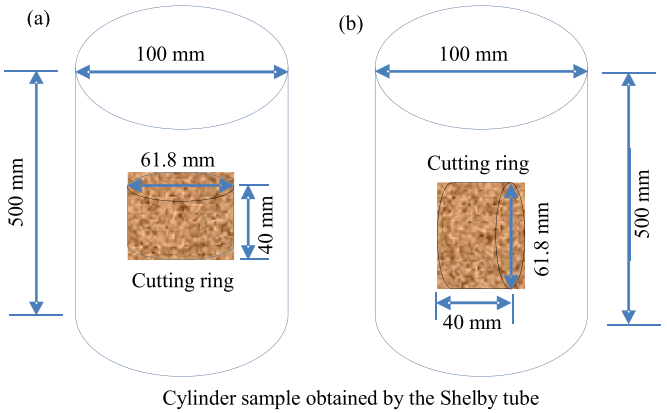

Fig. 2. Sampling method for permeability tests: (a) Longitudinal sampling and transverse sampling; and (b) Transverse sampling.

2.2. Test site construction

The air-boosted preloading system includes a vacuum preloading system and an air-boosted system, as shown in Fig. 1. The vacuum preloading system consists of different components, whose installation at the test site followed several steps:

(1) The woven geotextile was laid down to separate the drainage system from the dredged soil and to provide a platform for mobilizing construction equipment.
(2) The PVDs were manually rooted to a depth of 4.5 m in a square pattern with spacing of 1 m at both S1 and S2.
(3) The PVDs were extended 0.5 m above the ground and then tied to drainage branch tubes via hand-type connectors, and the other end of drainage branch tubes was connected to main vacuum tubes through four-way (or three-way) joints.
(4) The main vacuum tubes were joined to larger collecting pipes, through which pumped water was sent to an air-water separating tank by a vacuum pump.

(5) A peripheral ditch was dug around the test sections to contain the outflow, and a layer of geomembrane was placed over the ditch to prevent the water from seeping back into the ground.
(6) The wire hose was installed, above which two layers of vacuum geomembranes were placed. A layer of needle-punched geotextile was inserted between the wire hose and the lower layer of the geomembrane to prevent breakage of the vacuum geomembranes.

For the air-boosted system, the air injection pipe is the key component. To enhance the performance of the air-boosted system, we developed an innovative air injection pipe system, which includes steel wire wrapped with fabric, as shown in Fig. 1. The use of steel wire allowed the air injection pipe to resist bending and facilitated its installation. These injection pipes were inserted midway between the PVDs, and the injection spacing is 3 m to the same depth as the PVDs. Thereafter, their tops were connected to a booster pump and a plastic hose. By activating the booster pump, pressurized air was generated and injected through the injection pipes to the soil. However, air injection did not start until 40 d of vacuum preloading. Air injection was maintained for 20 d at an air pressure of 200 kPa. While the air was injected, vacuum preloading continued; therefore, vacuum loading was performed for 60 d in total. For conventional vacuum preloading that involved no air injection, the loading duration was also 60 d.

2.3. Monitoring plan

Field monitoring was implemented to evaluate the performance of the two vacuum preloading methods for improving the soils at the test sections. The ground settlement at the four corners and the center of each section was investigated every 3–5 d. Vacuum gages were installed to monitor the vacuum pressure under the geomembranes and to control the vacuum pressure. Vane shear tests were conducted before and after vacuum preloading to assess the changes in soil strength. Locations of the settlement measurement, the vacuum gages, and the vane shear tests are shown in Fig. 1.

2.4. Monitoring results

Fig. 3 shows the changes in the ground settlement during the 60-d vacuum preloading in both sections S1 and S2. Under the conventional vacuum preloading, the ground settlement reached 390 mm after 40 d, and it increased to 401 mm after 60 d. Under the air-boosted vacuum preloading, the ground settlement was 392 mm after 40 d, which was similar to that under the conventional vacuum preloading; however, the settlement was increased to 448 mm after 60 d, approximately 12% greater than that under the conventional vacuum preloading. Such an increase in the settlement indicates the benefit of the air-boosted vacuum preloading in accelerating consolidation.

Vane shear tests were performed to evaluate the changes in the undrained shear strength at six locations with distances of 0.1 m, 0.25 m and 0.5 m from the air injection pipe for S2 and from the PVDs for S1 (Fig. 1). Fig. 4 depicts the profiles of the undrained shear strength of soil before and after vacuum preloading. In general, the in situ soil undrained shear strength increased linearly with depth. After the vacuum preloading, the undrained shear strength increased within the depth of improvement (i.e. the upper 4.5 m); however, the noticeable increase took place in the upper 0.5 m. Moreover, the undrained shear strength increased more for the soil closer to the air injection pipes (in S2) or the PVDs (in S1), where the increase was more significant in the vicinity of the air injection

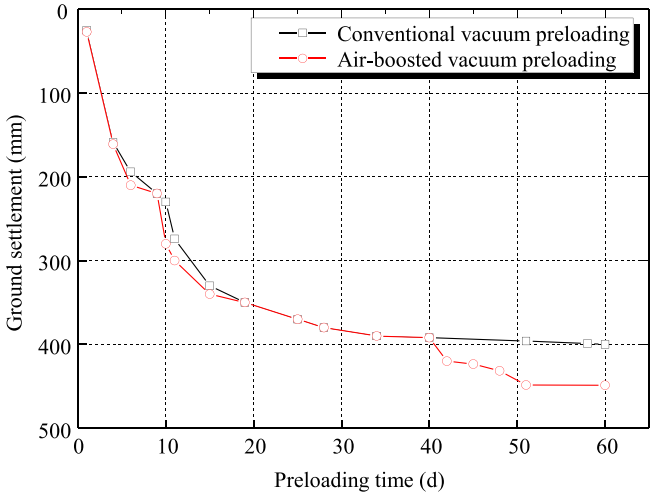

Fig. 3. Ground settlement by conventional and air-boosted vacuum preloading.

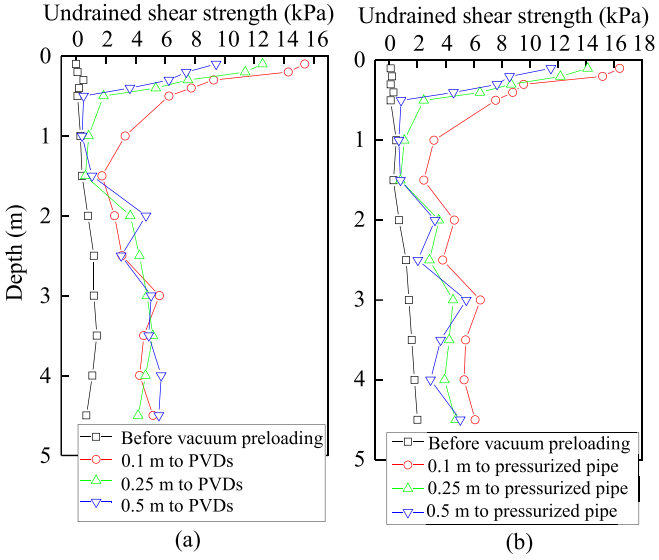

Fig. 4. Profiles of undrained shear strength before and after vacuum preloading: (a) S1 and (b) S2.

pipes than that surrounding the PVD pipes. For example, in S2, the undrained shear strengths at a depth of 0.1 m below the initial ground surface measured at distances of 0.5 m, 0.25 m and 0.1 m to the injection pipe were 11.5 kPa, 14.1 kPa and 16.3 kPa, respectively. In contrast, in S1, the undrained shear strengths at the same depth measured at distances of 0.5 m, 0.25 m, and 0.1 m to the PVD pipe were 9.4 kPa, 12.6 kPa and 15.4 kPa, respectively. This result confirms that the use of combined air injection and vacuum preloading further accelerates consolidation compared with vacuum preloading alone.

3. 2D continuum FE analyses

3.1. Baseline models

Baseline FE models were developed to simulate the field tests in S1 and S2. For the baseline FE models, the following assumptions were made:

(1) The vacuum pressure and air injection pressure were simulated as a negative and a positive pore water pressure, respectively.
(2) The test sections were simulated with a plane strain model.

A commercial FE software package, Plaxis 2D, was employed to develop both the conventional and air-boosted vacuum preloading models, as shown in Fig. 5. Due to the symmetry of the numerical model, only half the model was built. The boundaries were set at 32 m from the center and 16 m below the ground surface (Fig. 5), to adequately avoid the boundary effects on the numerical modeling. The vacuum preloading area in the numerical model was 7.5 m × 4.5 m (i.e. half the size of the field test section). There were eight PVDs in S1 and eight PVDs plus three air injection pipes in S2. The PVDs and air injection pipes were 4.5 m deep, the PVD spacing was 1 m, and the injection pipe spacing was 3 m. In the FE analyses, the PVDs and injection pipes were modeled as drain line elements in Plaxis 2D. The soils were modeled as an elastoplastic material using the hardening soil (HS) model in Plaxis 2D. The HS model is a second-order hyperbolic elastoplastic constitutive model, which can consider the large irreversible deformation of soft clay under compression (Liu et al., 2017b; Saleh et al., 2021). The constitutive model is suitable for the calculation and analysis of soft soil ground treated by vacuum preloading.

The soil parameters in the HS model mainly include the cohesion c, the friction angle φ, the compression modulus E, and the power parameter m that is dependent on soil rigidity and stress state. The parameters c and φ are determined by laboratory testing. The secant modulus E_{50}^{ref} and the loading-unloading stiffness $E_{\mathrm{ur}}^{\mathrm{ref}}$ are measured from CD triaxial tests, and the tangent modulus $E_{\mathrm{oed}}^{\mathrm{ref}}$ is measured from odometer tests. In our tests, the unloading modulus was not determined; therefore, the following equations were used to estimate these moduli (Schanz et al., 1999):

$$E_{50}^{\mathrm{ref}} \approx E_{\mathrm{ur}}^{\mathrm{ref}} \Big/ 3 \tag{1}$$

$$E_{50}^{\mathrm{ref}} \approx E_{\mathrm{oed}}^{\mathrm{ref}} \tag{2}$$

$$E_{\mathrm{oed}}^{\mathrm{ref}} \approx E \tag{3}$$

All the parameter values are listed in Table 1. The power parameter m, which characterized the degree of softness, was set to 1 since the softer the soil, the closer the parameter m to 1. The Poisson's ratio of soils was chosen according to the results presented by Gangaputhiran et al. (2016).

The soils were simulated as an assemblage of triangular FEs, with the mesh density set to "medium" in Plaxis 2D. Fifteen-node triangular elements are selected, which can ensure the accuracy of the calculation results. In total, there were 1151 elements and 9419 nodes in the conventional vacuum preloading model and 2242 elements and 18,229 nodes in the air-boosted vacuum preloading model. The boundary was fixed at the bottom but free on the top. Both the left and right boundaries were fixed in the horizontal direction but free in the vertical direction. The FE analysis employed a fully implicit time-marching scheme, enabling the large-strain consolidation to be evaluated. The calculation of large-strain deformation was based on a Lagrangian formulation that updates the FE mesh and the stiffness matrix at the beginning of each iteration (Indraratna et al., 2016).

The conventional vacuum preloading process was simulated in three construction phases in Plaxis 2D. The initial phase was used to establish the k_0-state equilibrium in the model, with the k_0 values given in Table 1. The second phase was activated to impose a vacuum pressure of 90 kPa for 10 d. In this phase, the vacuum pressure rose linearly to the target value of 90 kPa, and any deficiency such as vacuum geomembrane leakage or sensor damage was noted by field inspection. Note that the FE model could not simulate these deficiencies while the second phase was set up in the FE model to be consistent with the field loading process. In the final phase, vacuum preloading continued for another 50 d. For the air-boosted vacuum preloading, four construction phases were created. The first and second phases were the same as those for the conventional vacuum preloading. In the third phase, the vacuum preloading was continued for another 30 d, and the final phase imposed air injection with an air pressure of 200 kPa while maintaining the vacuum preloading for 20 d.

3.2. Model validation

The numerical analysis results were compared with the field monitoring data to validate the FE models. Fig. 6 depicts the ground settlement determined by both FE analyses and field monitoring. Fig. 6a plots the settlement–time curves under conventional vacuum preloading. In general, the settlement trend and the 60th day settlement obtained from both FE analyses and field monitoring were similar. However, there was a remarkable discrepancy (a difference of approximately 62%) between the measured and calculated values at the 10th day of vacuum preloading. This is because the FE model used constant hydraulic conductivity while in the field, this value may be reduced by the increased pressure. The first 10 d of construction was the trial phase for vacuum preloading in engineering

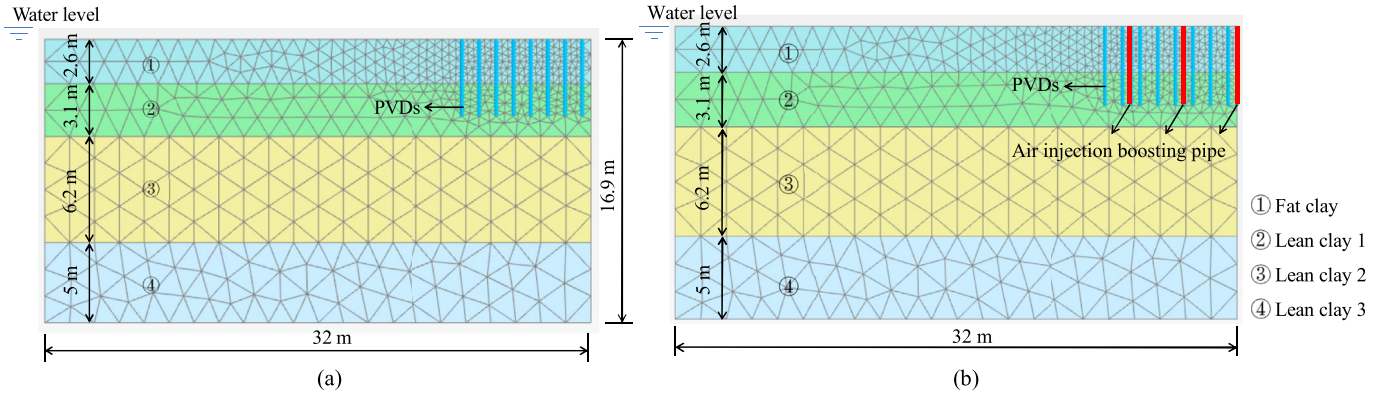

Fig. 5. FE baseline models: (a) Conventional vacuum preloading; and (b) Air-boosted vacuum preloading.

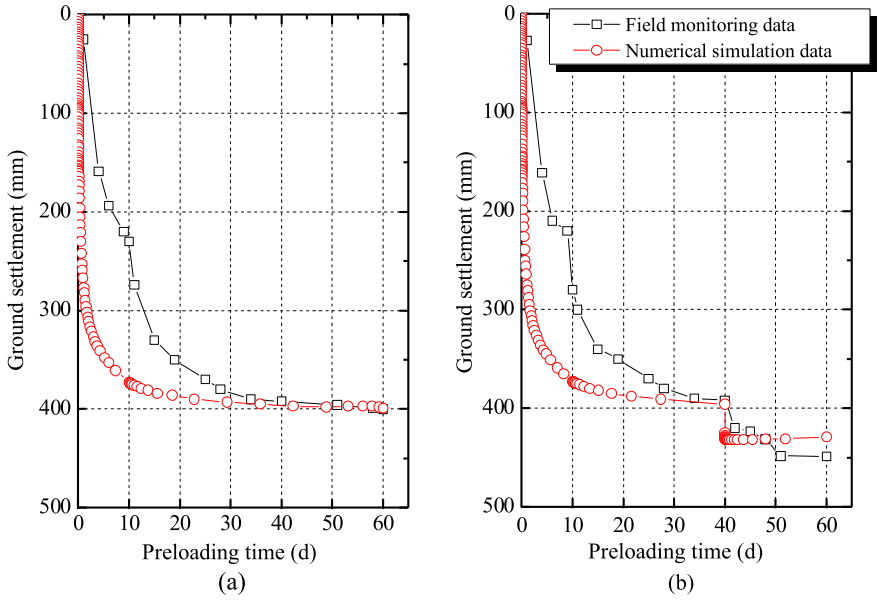

Fig. 6. Settlement at different preloading times: (a) Conventional vacuum preloading; and (b) Air-boosted vacuum preloading.

practice, and the monitoring data were incomplete because tightness of the vacuum membrane should be double-checked. Beyond this stage, the vacuum pressure tended to be stable. When the vacuum preloading time was 60 d, the minimum discrepancy between field monitoring results and numerical simulation data of the conventional vacuum preloading method was 2.3%. Fig. 6b shows variations of the ground settlement with time under air-boosted vacuum preloading. The ground settlements during the air injection (i.e. between the 40th and 60th day) from FE analyses and field monitoring were comparable, but the consolidation rate was higher in the FE modeling than in the field monitoring. As discussed previously, this might be because the injected air pressure decreases the hydraulic conductivities with time in the field. However, the minimum error of the settlement corresponding to the 45th day was the smallest, approximately 3.56%. The above comparisons indicate that the baseline large-strain FE models were able to simulate both vacuum preloading processes. The baseline FE models were thus further utilized for the parametric analyses of the air-boosted vacuum preloading, considering the effects of key influencing factors, i.e. different injection pressures, injection spacings, and injection cycles and durations, as discussed in the following sections.

3.3. FE parametric analyses for air-boosted vacuum preloading

The key factors influencing the effectiveness of air-boosted vacuum preloading were investigated with the FE models. At present, there is no consensus on the selection of a proper range of air injection pressures. Some researchers recommended that the injection pressure should be no more than 100 kPa, while others suggested that the pressure should be in excess of 100 kPa. Based on the monitoring data, Wang et al. (2016) and Cai et al. (2018) found that air-boosted vacuum preloading was most effective when the injection pressure was 80 kPa, while Anda et al. (2020) indicated that a lower range of the injection pressure, i.e. 0–20 kPa, was preferable. Based on field tests, Shen et al. (2015) observed that the preferable air injection pressure was 400 kPa. Xie et al. (2009) found that when the injection pressure ranged between 60 kPa and 200 kPa, the drainage efficiency was improved as the air injection pressure increased.

In the FE parametric analyses, eight air injection pressures, ranging from 50 kPa to 350 kPa with continuous air injection for 20 d and injection spacing of 3 m, were selected to determine the optimum air injection pressure. At an air injection pressure of 200 kPa with continuous air injection for 20 d, four injection spacings ranging from 1 m to 4 m were evaluated. Air injection in a cyclic manner (square shape in Fig. 7) was also investigated with injection spacing of 3 m, an amplitude of 200 kPa, cyclic numbers of $N = 1$, 2, 4 and 5, and various injection periods, $2T$, where T is the injection time per cycle, equal to 1 d, 2 d and 3 d.

3.4. Results of the parametric analyses for air-boosted vacuum preloading

Fig. 8 shows the locations (Points a_1–a_3, b_1–b_3, c_1–c_3 and e_1–e_3) at which the FE numerical results were extracted from the FE analyses. The center points c_1–c_3 were monitored for ground settlement and soil lateral movement. Points a_1–a_3 and b_1–b_3 were surveyed for ground settlement, the evolution of the ground settlement and the lateral displacement at different depths. Vertical and lateral displacements of soils at Points e_1–e_3 were monitored to evaluate the influence of vacuum preloading on the soils outside the improvement area. The horizontal distances e_1 to a_1, a_1 to b_1, and b_1 to c_1 were 5 m, 4 m and 3.5 m, respectively, and the vertical distance between the neighboring monitoring points was 2.25 m.

3.4.1. Effects of air injection pressures

The results of the vertical and lateral displacements of soils were calculated with the FE models to evaluate the effects of air injection pressure on soil consolidation.

(1) Ground settlement

Fig. 9 presents the ground settlement (or vertical displacement at c_1) under different air injection pressures.

Based on the characteristics of the settlement curves, we divided the settlement into two stages. Stage I was the first 40 d when only vacuum preloading was applied, while Stage II referred to the period between the 40th and 60th day when both vacuum

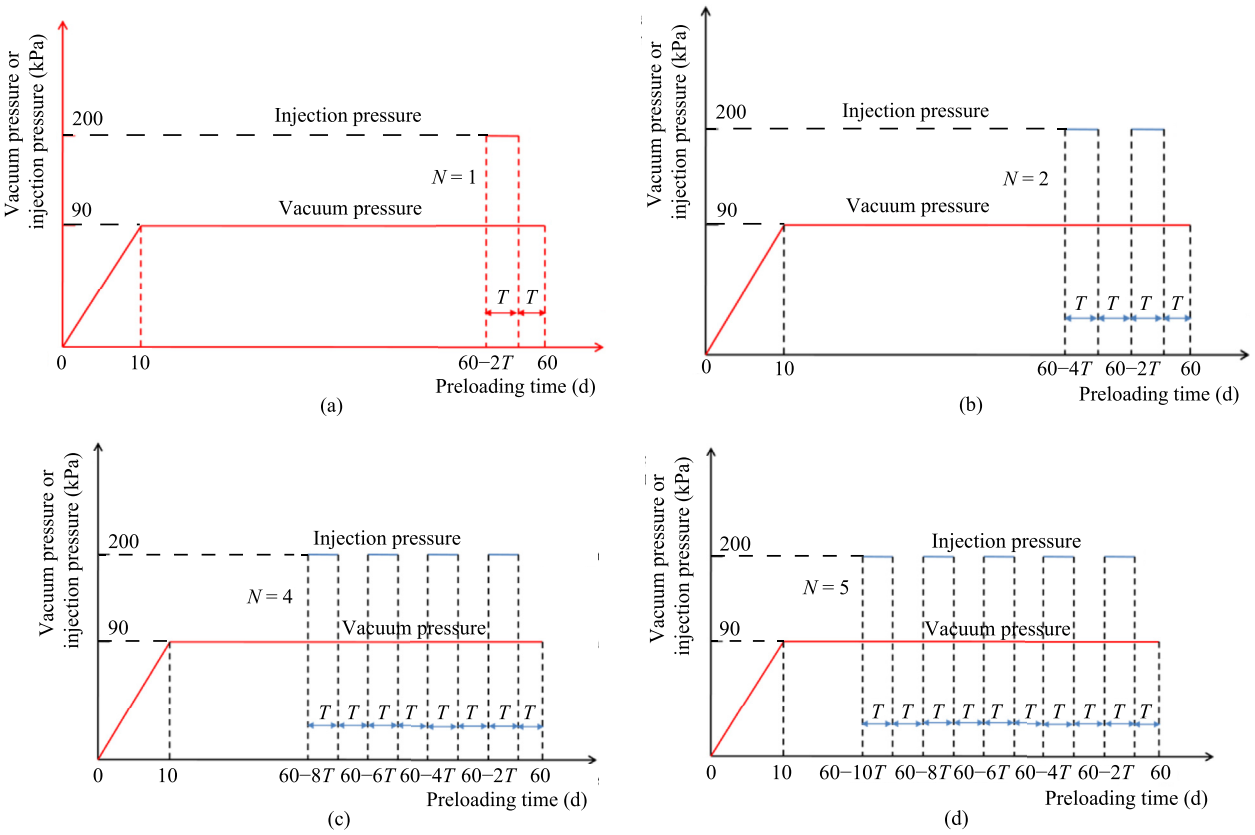

Fig. 7. Twelve intermittent types of air injection in the FE analyses: (a) $N = 1$, with injection duration of $2T$; (b) $N = 2$, with injection duration of $4T$; (c) $N = 4$, with injection duration of $8T$; and (d) $N = 5$, with injection duration of $10T$. $T = 1$ d, 2 d and 3 d. N is the number of injection cycles, T is the injection time per cycle, and $2T$ is the injection period.

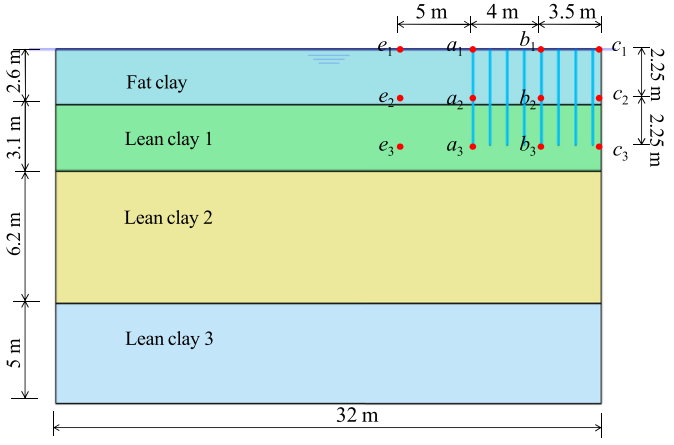

Fig. 8. Positions at which numerical results were obtained.

preloading and air injection were imposed. The ground settled 396 mm at the end of Stage I, and the settlement rapidly increased once the air pressures were applied at the beginning of Stage II. Overall, the ground settlement increased with an increase in air injection pressure. The settlement increase in percentage resulting from air injection followed a logarithmic relation with air injection pressure, as shown in Fig. 9b. At a lower injection pressure, the settlement progressively increased with time (see the inset of Fig. 9a); however, at a higher injection pressure, the settlement rapidly jumped to the maximum upon the application of pressure, followed by a slight rebound. This might be because the higher injection (positive) pressure compromised the vacuum pressure, reducing the efficiency of the vacuum loading. The contour of excess pore water pressure was plotted to explain the slight rebound of the ground, as shown in Fig. 9c. The magnitude of negative excess pore water pressure was not altered much upon the application of high air injection pressure (i.e. 350 kPa at the 40th day) but decreased after the high injection pressure was maintained for a certain time (i.e. 350 kPa at the 60th day). In contrast, the magnitude of negative pore water pressure at a lower injection pressure did not change much with a change in injection time (i.e. 50 kPa at the 40th day vs. 50 kPa at the 60th day). This phenomenon was consistent with the results reported by Ke et al. (2020). The above FE analysis result also indicates that when the air injection pressure was higher than 100 kPa, a longer duration of continuous air injection might not necessarily be beneficial.

The inset of Fig. 9a shows the ground settlement at Point c_1, while the ground settlement data for other locations (i.e. Points a_1, b_1, c_1 and e_1), at the beginning and end of the air injection, are plotted in Fig. 10, and the regression relation is also shown in the figure. It was observed that the ground settlement decreased nonlinearly with the horizontal distance to the center of the treated area. Moreover, the decreasing rate was more pronounced at higher injection pressure. Fig. 10 also indicates that variations of ground settlement due to the varied injection pressures were noted at a_1 but disappeared at e_1, which indicated that the influence of air injection reached but was not beyond the edge of the improvement area.

(2) Lateral displacement

Many studies have indicated that the application of vacuum pressures could induce lateral movement of soil toward the center of the improvement area (i.e. inward displacement), and a larger lateral displacement leads to better ground improvement (Griffin and O'Kelly, 2014; Shibata et al., 2014; Cai et al., 2018). Therefore, lateral displacement of soils due to vacuum pressures was investigated in the FE analyses, and lateral displacement to the right (relative to Point c_1) was positive, and negative otherwise. Fig. 11 depicts the calculated lateral displacement at the edge of the improvement area (i.e. Point a_1) under different air injection pressures. In Stage I, the lateral displacement increased over the vacuum preloading time and gradually stabilized after 10 d. The maximum lateral displacement at Point a_1 was approximately 90 mm in this stage. In Stage II, the lateral displacement was further increased and reached the maximum on the 42nd day. The maximum values ranged from approximately 97 mm–119 mm corresponding to a higher injection pressure. The lateral displacement generally stabilized when the air injection pressure was less than 100 kPa but rebounded at a pressure greater than 100 kPa, which was similar to the trend of the ground settlement. The lateral displacement at the end of Stage II ranged from 97 mm to 114 mm. In general, the lateral displacement at ground surface was approximately 28%–33% of the ground settlement under the air-boosted vacuum preloading.

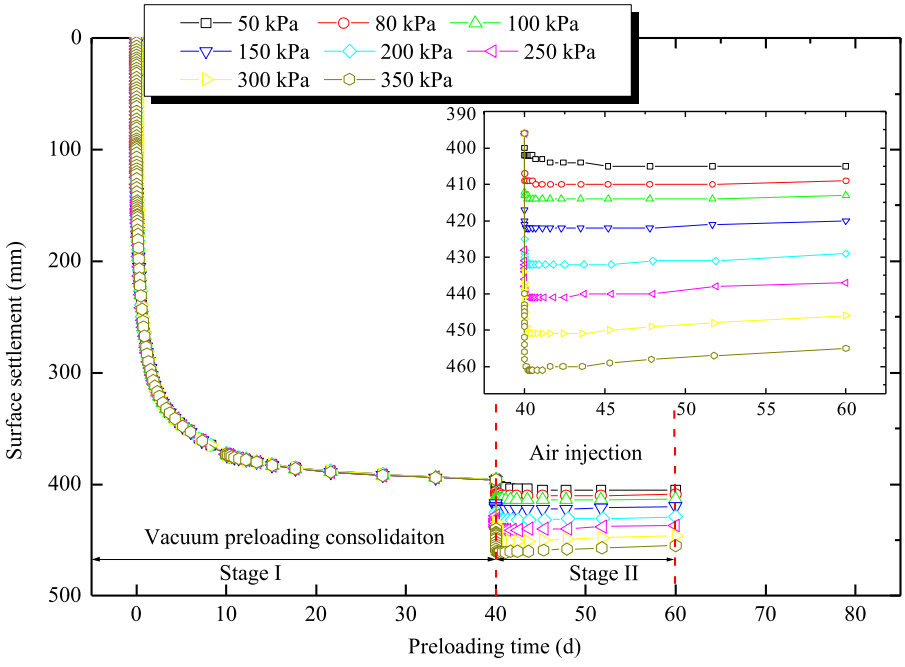

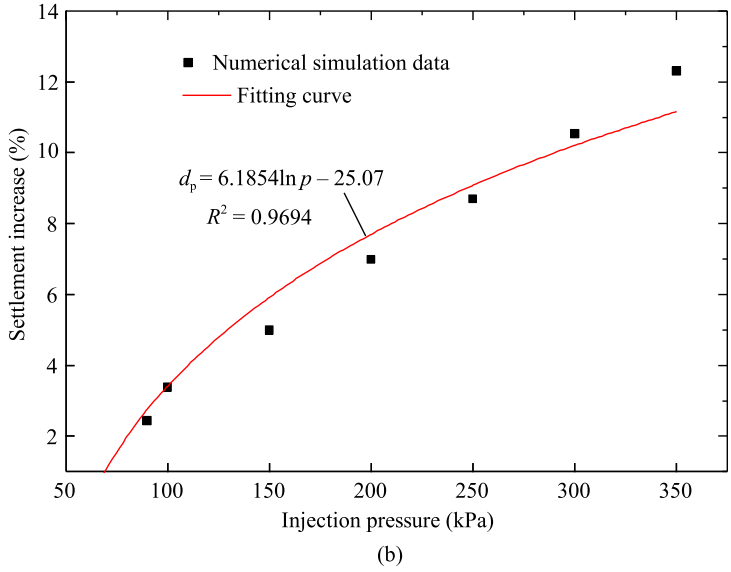

Fig. 9. Ground settlements and excess pore water pressures under different air injection pressures: (a) Evolution of the surface settlement; (b) Percent increase in the ground settlement; and (c) Contour of the excess pore water pressure.

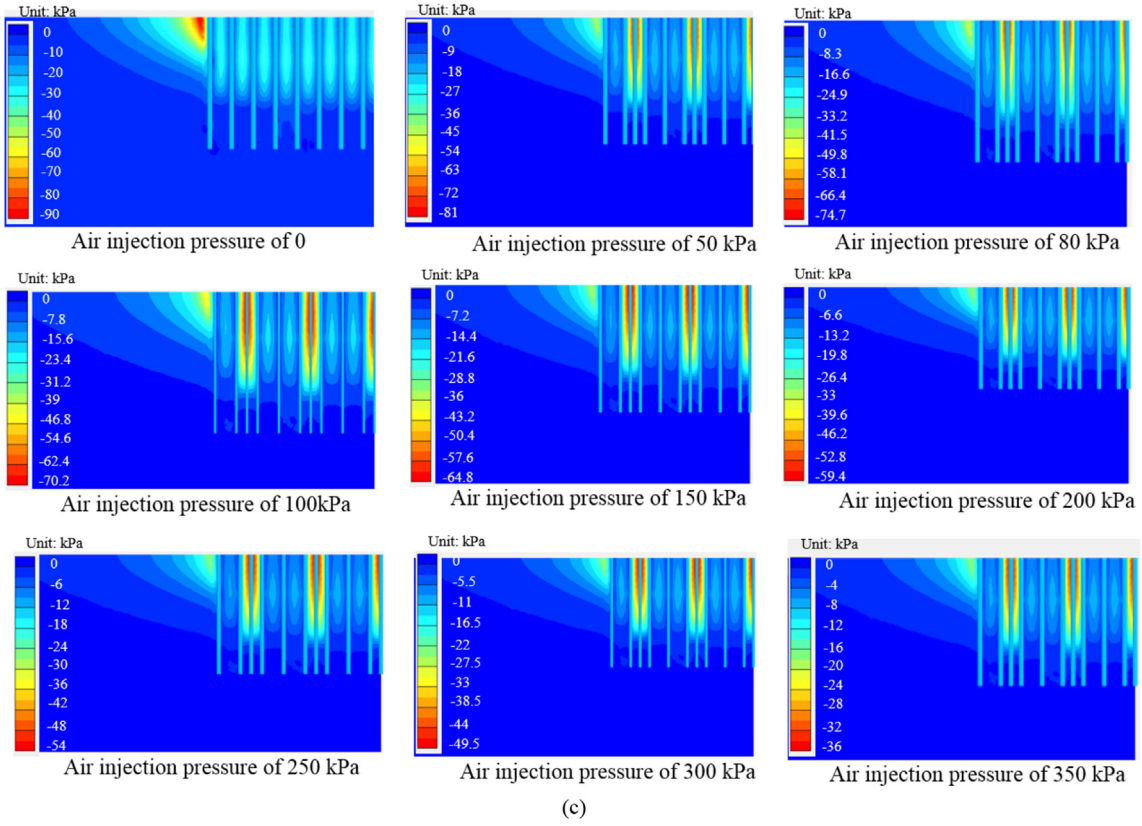

(c)

Fig. 9. (*continued*).

3.4.2. *Effects of injection spacing*

The effect of injection spacing was quantified by ground settlement and lateral displacement. The results are plotted in Figs. 12 and 13. Fig. 12a shows the variations of ground settlement with air injection spacing at Point c_1. Fig. 12b displays the ground settlement increase in percentage versus injection spacing, which followed a negative power relation. Compared with vacuum preloading with no air injection, the air injection (i.e. air-boosted vacuum preloading) increased the ground settlement by 18.3%, 10%, 7.5% and 7% for the injection spacing of 1 m, 2 m, 3 m and 4 m, respectively. This result indicates that ground settlement decreased more significantly for the spacing between 1 m and 3 m (inclusive) than that for the spacing greater than 3 m.

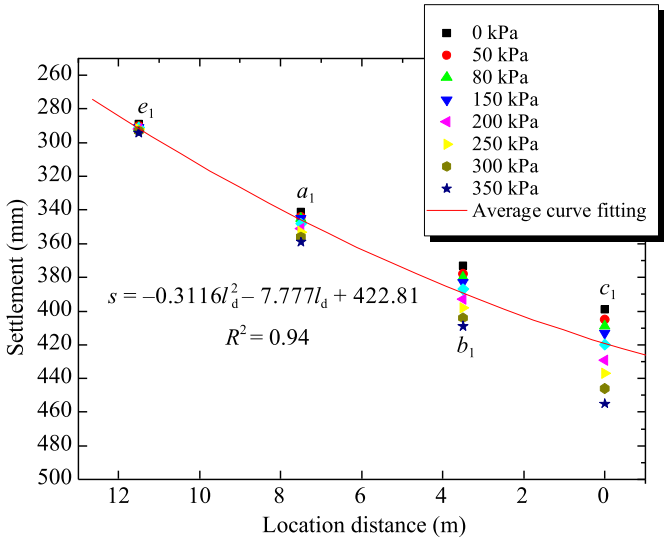

Fig. 10. Ground settlements at different locations on the ground surface under different injection pressures.

Fig. 13 illustrates the evolution of the lateral displacement of soils at various depths below the edge of the improvement area (i.e. Points a_1, a_2 and a_3) affected by different air injection spacings. In general, the lateral displacement was smaller at a greater depth (comparing a_1 with a_3), indicating the decreased effect of injection spacing with increasing depth; however, the trends of lateral displacement at different depths were generally similar. The maximum lateral displacement due to air injection occurred 1–2 d after the application of the air injection. This implied that to maintain a favorable treatment result, the duration of continuous air injection should not be less than 2 d when the injection pressure was 200 kPa; however, an overly long injection time (e.g. 10 d or longer) was not helpful either.

The maximum lateral displacement at a_1 due to the air-boosted vacuum preloading is plotted versus injection spacing and depth in Fig. 14. The relation between the maximum lateral displacement and the depth is a quadratic function, as shown in Fig. 14. The simulated results show that the air-boosted vacuum preloading technique could increase the lateral displacement, particularly at shallow depths. The uneven increase in the lateral displacement at different depths would cause the ground to crack and PVDs and injection pipes to bend. A proper monitoring program can be implemented to ensure that the lateral displacement is within the tolerable range for specific applications, where care may be taken

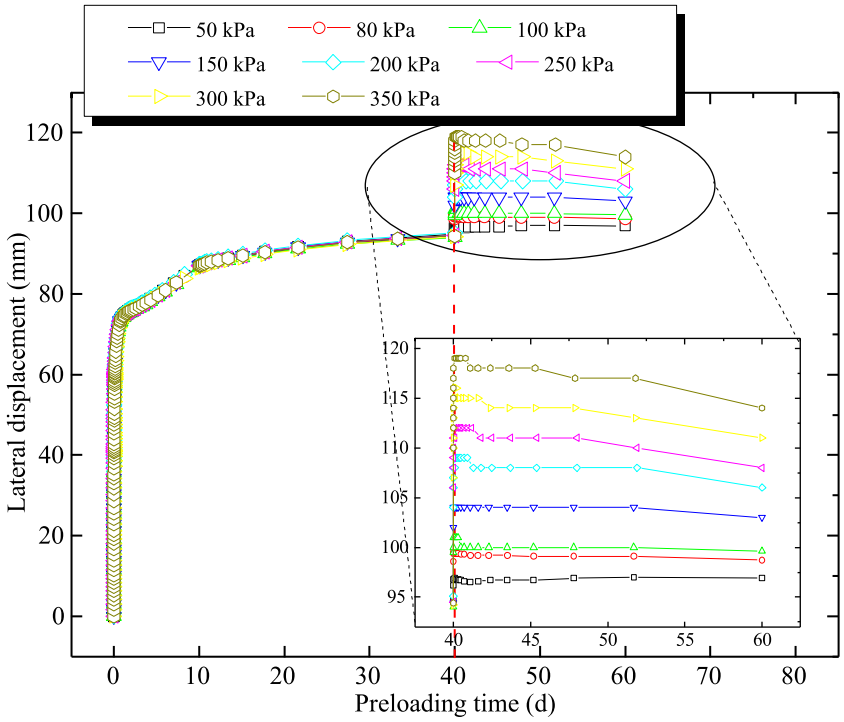

Fig. 11. Effects of air injection pressures on the lateral displacement at the edge of the improvement area (i.e. Point a_1).

to control the lateral movement of soils at the ground surface as the maximum lateral displacement occurs at shallow depths. In the preliminary design stage, when the monitoring program is unavailable, the lateral ground displacement may be estimated by multiplying the calculated ground settlement with an empirical factor, as discussed previously and shown in Table 2.

3.4.3. *Effect of cyclic air injections*

In the previous section, the data showed that continuous air injection for a longer duration might not be beneficial for ground improvement. Therefore, cyclic air injection, with $T = 3$ d and a square shape, was investigated under an air injection pressure of 200 kPa. The results are presented in Figs. 15 and 16. For comparison purposes, the injection with various periods (i.e. $2T$) was imposed with the same terminal time (i.e. the 60th day) but different starting times (see Fig. 7).

Fig. 15a shows that cyclic air injection led to an increased cumulative ground settlement, which is in contrast to the case with continuous air injection (e.g. Fig. 12) that would cause ground rebound. Note that this result was obtained under a high injection pressure of 200 kPa and an injection spacing of 1 m. For a similar duration of air injection, ground settlement due to the cyclic injection (438 mm for $N = 4$ in Fig. 15) was also larger than that induced by the continuous injection (432 mm under 200 kPa in Fig. 9). The above results imply that imposing longer cyclic air injection was beneficial to the development of settlement more than imposing continuous air injection when injection spacing, injection pressure, and injection duration were similar. In addition, the relation between settlement increase in percentage (d_{in}) and number of injection cycles (N) was established for various values of T, where T is the injection time per cycle or half the injection period, as shown in Fig. 15b. The intercept of lines in Fig. 15b represents the effect of T alone, and the value of the intercept in relation to T is plotted in Fig. 15c. In addition, the injection period ($2T$) effect was also evaluated by varying the value of T. In summary, the correlation between the settlement increase in percentage (d_{in}), N and T is as follows:

$$d_{in} = 0.01N + 0.015T + 0.98 \tag{4}$$

Eq. (4) is only applicable to $T = 1$ d, 2 d and 3 d.

Fig. 16a–c depicts the time-dependent lateral displacement with various injection cycles below the edge of the improvement area (i.e. Points a_1–a_3). In general, lateral displacement increased with increasing injection cycles but decreased with increasing depth (0 m, 2.25 m and 4.5 m). The lateral displacement on the 60th day was 7.3%–12.5%, 5.3%–8.4% and 0.9%–3% greater than that under conventional vacuum preloading at depths of 0 m, 2.25 m and 4.5 m, respectively. The development of lateral displacement at various depths is exhibited in Fig. 17, showing a progressive decrease with depth.

4. Development of the empirical settlement prediction equation

Based on the results of the field tests and the FE parametric analyses, we proposed a simple and practical closed-form expression to calculate the consolidation settlement under air-boosted vacuum preloading. The closed-form equation took the form of the existing methods for conventional vacuum preloading but improved it by considering the influencing factors of air injection. The proposed equation was then validated against a case history reported by others.

4.1. *Closed-form expression*

Several empirical solutions are available to predict consolidation settlement under conventional vacuum preloading, including the

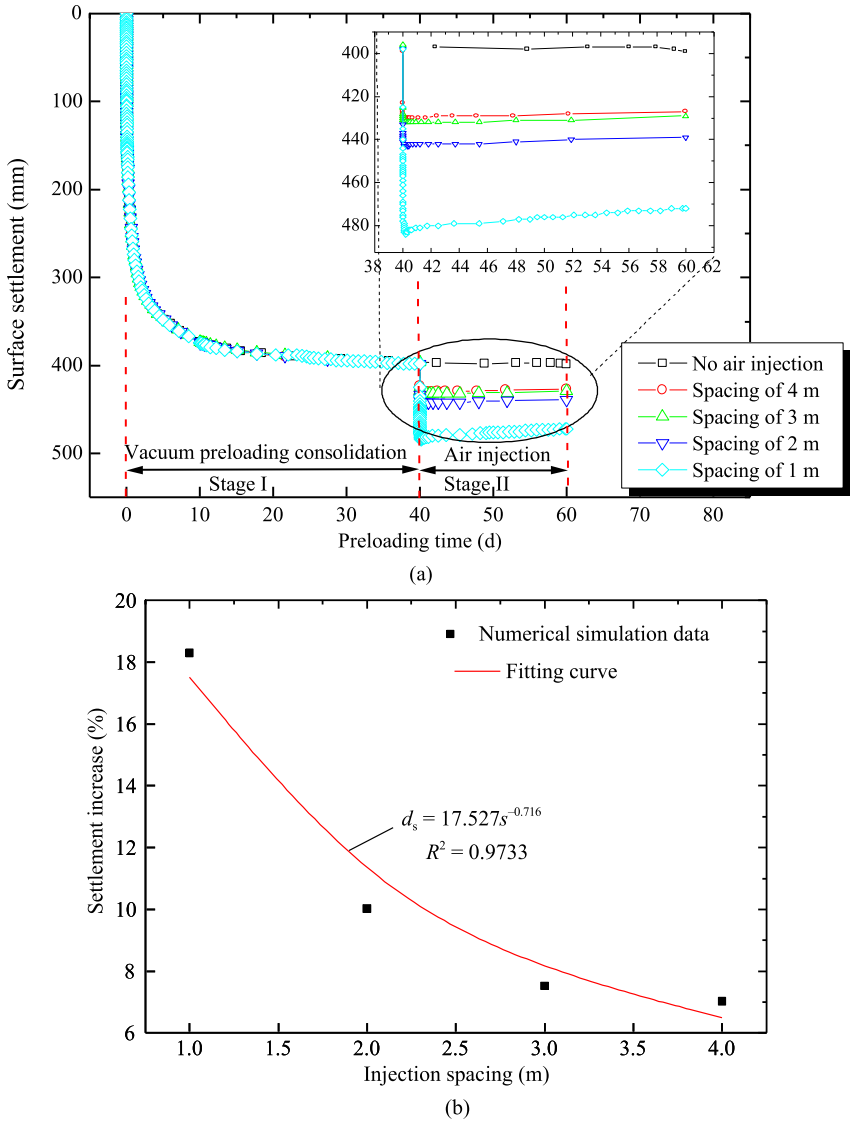

Fig. 12. Variations of ground settlement with injection spacing: (a) Evolution of the ground settlement; and (b) Percent increase in the ground settlement (injection pressure = 200 kPa).

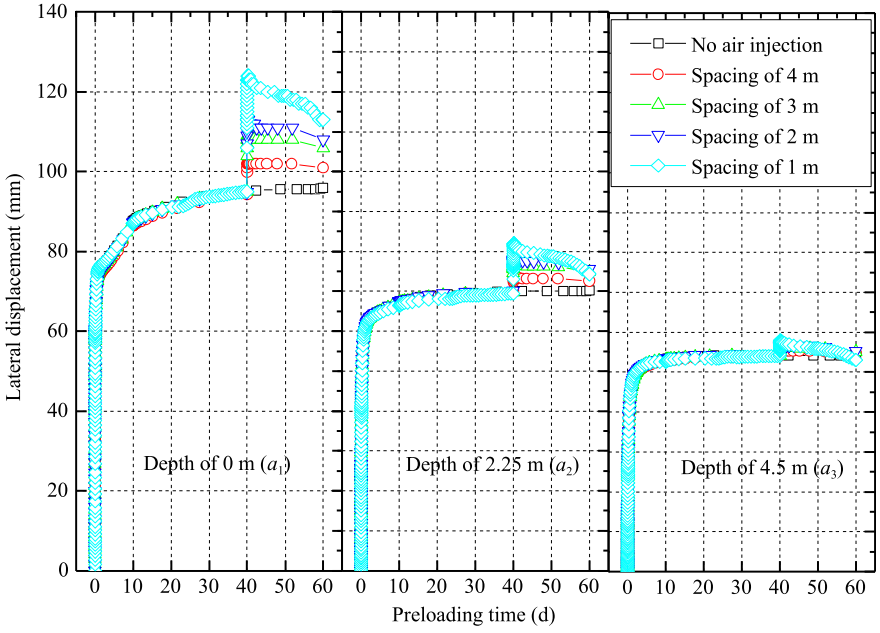

Fig. 13. Effects of injection spacing on the lateral displacement of soils at different depths below the edge of the improvement area (injection pressure = 200 kPa).

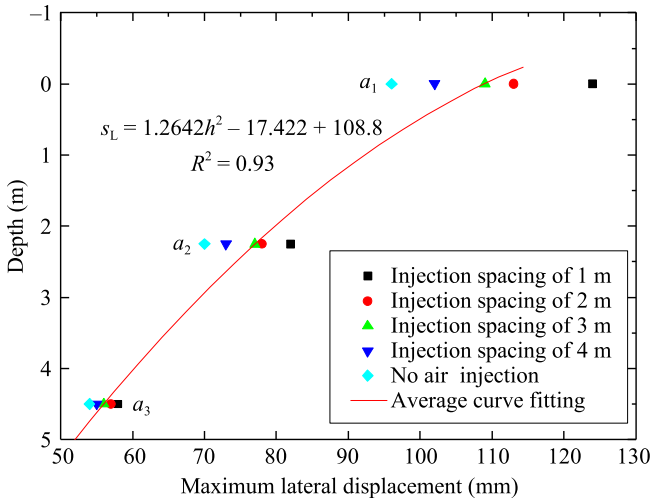

Fig. 14. Relation between the maximum lateral displacement and the depth.

Table 2
Empirical factor for predicting the lateral displacement.

Locations (surface position)	Empirical factor (%)				
	1 m	2 m	3 m	4 m	Infinity (no injection)
a_1	27.4 −34.2	26.5 −33.9	26.8 −33.8	26.4 −33.3	26.7–33.2
b_1	23.8 −28.7	23.5 −28.1	24.7 −30.3	23.3–28	24.8–30.2
c_1	22.9 −27.1	22.9 −26.9	23.1 −27.3	22.6 −26.6	23.1–27.1

three-point method (Zheng et al., 2017), the hyperbolic method (Uy and Dungca, 2018), the logistic regression method (Goh et al., 2017), and the Chinese standard method (JTS 147–2–2009, 2009).

The three-point method takes the following form and is used to predict long-term settlement:

$$s_t = s_d\alpha^* e^{\beta^* t} + s_\infty\left(1 - \alpha^* e^{-\beta^* t}\right) \tag{5}$$

where s_d is the immediate consolidation settlement (mm), which is typically ignored and taken as zero in the vacuum preloading; s_t is the consolidation settlement (mm) at time t; t is the vacuum preloading time (d); and s_∞ is the ultimate consolidation settlement. Eq. (6) is adopted to determine where three random points ((t_1, s_1), (t_2, s_2), and (t_3, s_3)) with equal time interval ($t_3 - t_2 = t_2 - t_1$) are selected from the measured settlement curve in the short term. This means that the three-point method is suitable to predict the settlement during the construction process instead of the design. In these equations, α^* and β^* are empirical parameters, which are respectively determined by Eqs. (7) and (8) as follows:

$$s_\infty = \frac{s_3(s_2 - s_1) - s_2(s_3 - s_2)}{(s_2 - s_1) - (s_3 - s_2)} \tag{6}$$

$$\alpha^* = \frac{(s_3 - s_2)(t_3 - t_1)(t_2 - t_1)}{(s_3 - s_1)(s_2 - s_1)(t_3 - t_2)} \tag{7}$$

$$\beta^* = \frac{(t_3 - t_1)(s_2 - s_1) - (t_2 - t_1)(s_3 - s_1)}{(s_3 - s_1)(s_2 - s_1)(t_3 - t_2)} \tag{8}$$

The hyperbolic method uses the hyperbolic equation to predict the ground settlement as follows:

$$s_t = s_0 + \frac{t - t_0}{\alpha + \beta(t - t_0)} \tag{9}$$

where s_0 is the consolidation settlement (mm) corresponding to the time t_0 (d) when vacuum preloading begins, and if $t_0 = 0$, then $s_0 = 0$; and α and β are the parameters related to the slope and ultimate value of the settlement–preloading time curves, respectively, i.e. $\alpha = \Delta t/\Delta s_t$ and $\beta = 1/s_\infty$. α and β can be back-calculated from the field test data; however, when the field test data are not available, their values may be obtained based on the consolidation theory. The value of β may be determined according to Lei et al. (2019) as follows:

$$\beta = \frac{1}{\sum_{i=1}^{n} \xi h_i(e_{0i} - e_{1i})/(1 + e_{0i})} \tag{10}$$

where e_{0i} is the void ratio before vacuum preloading; e_{1i} is the void ratio after vacuum preloading, which is estimated as approximately 0.6–0.7 times the initial void ratio; h_i is the thickness of the ith soil layer or the depth of the improvement (mm); and ξ is an empirical coefficient, equal to 1.1–1.4 (Shen et al., 2015; Feng et al., 2021).

The estimation of α may be linked to the average degree of consolidation, U_a, as follows:

$$\alpha = \chi\left(\frac{t}{U_a} - t\right) \tag{11}$$

where χ is an empirical coefficient for different average consolidation degrees, which may be estimated using $\chi = 6\times10^{-12}e^{23.578U_a}$; and U_a may be specified by the project requirement or calculated using the standard method as discussed later.

The logistic regression method given in Eq. (12) involves three empirical parameters b_1, b_2 and b_3, which are back-calculated from field tests or numerical simulations.

$$s_t = \frac{b_1}{1 + b_2 e^{-b_3 t}} \tag{12}$$

The standard method is stipulated by the Chinese standard (JTS 147–2–2009, 2009), which equates the PVD with a sand well and specifies procedures for the calculation of the average degree of consolidation, U_a, as follows:

$$s_t = U_a s_\infty \tag{13}$$

$$U_a = 1 - \exp\left(-\frac{8C_h t}{F(n)d_e^2}\right) \tag{14}$$

$$\left.\begin{aligned} F(n) &= \frac{n^2}{n^2 - 1}\ln n - \frac{3n^2 - 1}{4n^2} \\ n &= d_e/d_w,\ d_e = \alpha_1 d \\ d_w &= \alpha_2[2(b + \delta)]/\pi \end{aligned}\right\} \tag{15}$$

where δ and b are the thickness and width of the PVDs, respectively; α_1 and α_2 are the empirical coefficients, of which α_1 is taken as 1.13 for square arrangement patterns of PVDs, and α_2 as 1 when laboratory experimental data are unavailable; and C_h is the horizontal coefficient of consolidation.

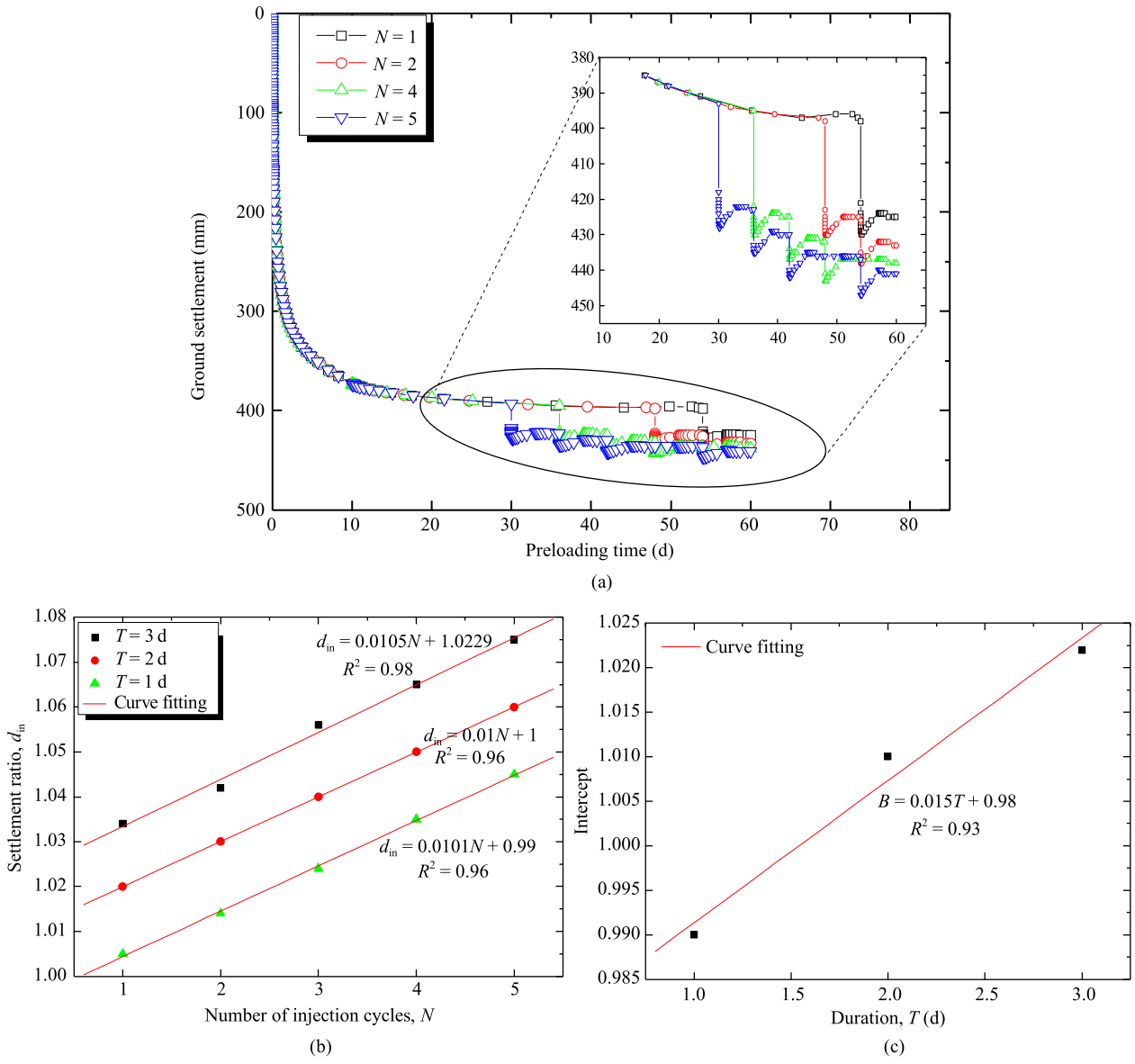

Fig. 15. Evolution of the ground settlement under different cyclic air injection schemes: (a) Settlement versus the preloading time for different numbers of air injections; (b) Relation between the increasing degree of settlement and the intermittent air injection number; and (c) Relation between the duration and the intercept.

With the previously suggested methods, the ground settlement of the project site under vacuum preloading (without air injection) was estimated and compared with the field test data. All the parameters used for these methods are summarized in Table 3. The results are plotted in Fig. 17. In comparison to the field monitoring data, the hyperbolic method gave the best estimate among the four methods. Therefore, the hyperbolic equation was further utilized to derive a closed-form expression for the case of air-boosted vacuum preloading by incorporating the influencing factors, i.e. the injection pressure, the injection spacing, and the characteristics of cyclic injection as follows:

$$s_{tc} = s_c(1 + d_p)(1 + d_s)d_{in} \tag{16}$$

where s_{tc} is the consolidation settlement of soil under combined air injection and vacuum preloading; s_c is the consolidation settlement with vacuum preloading alone, which can be determined by Eq. (9); d_{in} is the settlement increases in percentage (settlement ratio) considering the injection cycle and period, and can be calculated using Eq. (4); and d_p and d_s are the settlement increases in percentage considering effects of injection pressure and injection spacing, respectively, which can be obtained using Eq. (17) (corresponding to Fig. 9b) and Eq. (18) (corresponding to Fig. 12b).

$$d_p = 6.1854 \ln p - 25.07 \tag{17}$$

$$d_s = 17.527 s^{-0.716} \tag{18}$$

where p is the injection pressure (kPa), which is limited in the range of 50–350 kPa; and s is the air injection spacing (m) ranging from 1 m to 4 m.

To summarize, the calculation of the consolidation settlement of air-boosted vacuum preloading involves three steps. First, α and β are determined using Eqs. (11) and (10), respectively, during which Eqs. (14) and (15) will be invoked to determine α. Once these two parameters are determined, Eq. (9) is used to calculate the consolidation settlement from vacuum preloading alone. Second, d_p, d_s and d_{in} are determined using Eqs. (17), (18) and (4), respectively. Finally, the proposed closed-form equation (i.e. Eq. (16)) is

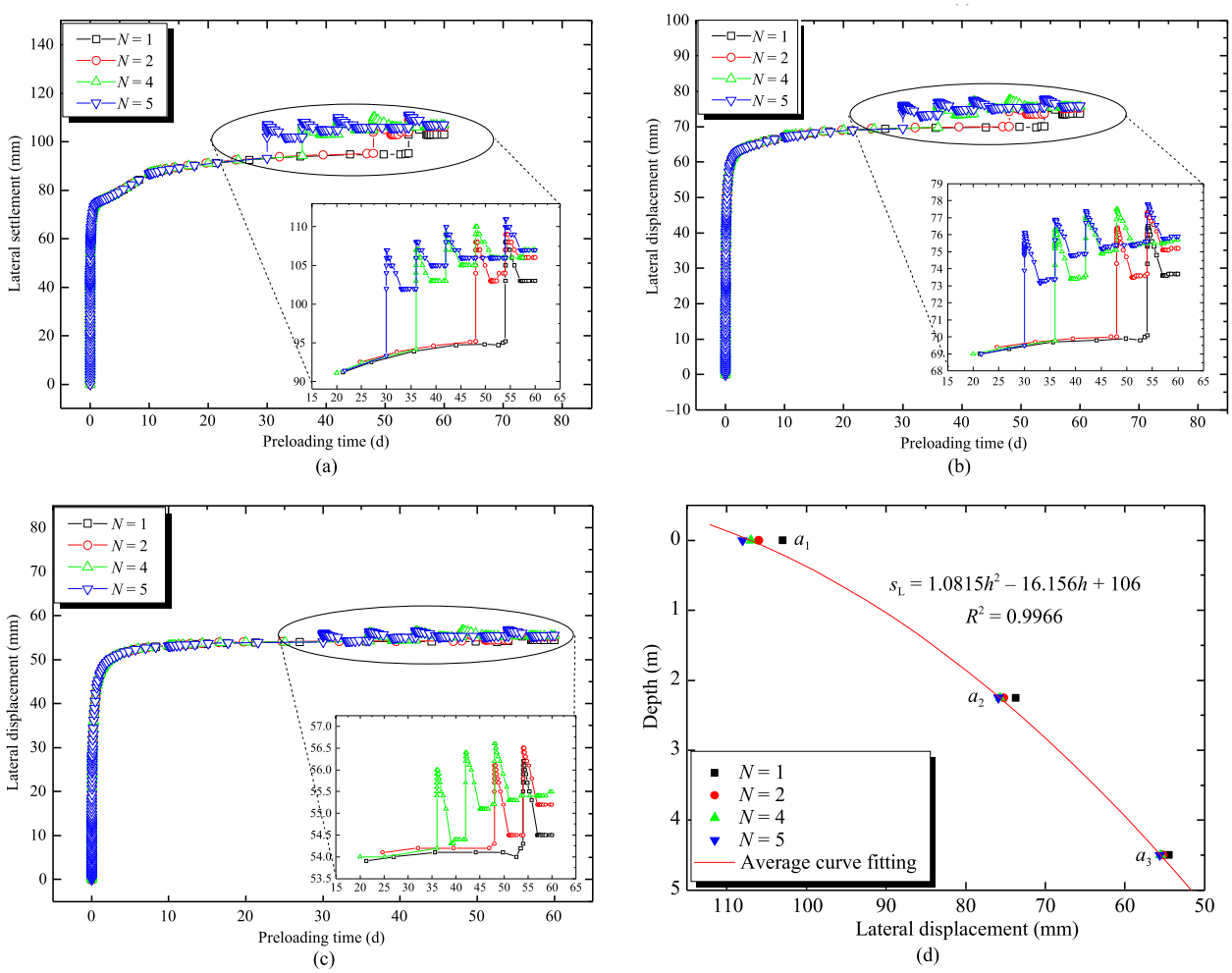

Fig. 16. Lateral displacement versus the preloading time for different numbers of air injection cycle at depths of (a) 0 m, (b) 2.25 m, and (c) 4.5 m; and (d) Lateral displacement versus depth relation.

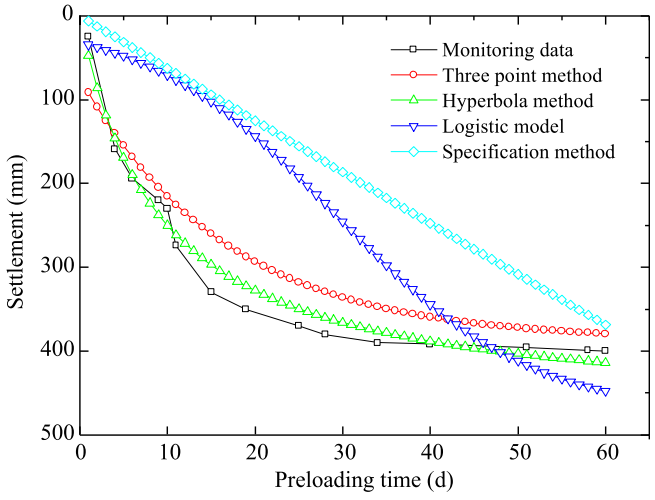

Fig. 17. Vacuum preloading induced ground settlement estimated by four empirical methods.

Table 3
Parameters for different empirical methods.

Three-point method					
(t_1 (d), s_1 (mm))	(t_2 (d), s_2 (mm))	(t_3 (d), s_3 (mm))	α^*	β^*	s_∞ (mm)
(50, 396)	(55, 397)	(60, 400)	7.5	−0.5	395.5
Hyperbolic method					
t_0	s_0	α		β	
0	0	0.0199		0.0021	
Logistic regression method					
b_1		b_2		b_3	
3.87×10^2		6.6		2.49×10^{-1}	
Specification method					
C_h (cm^2/s)	α_1	α_2	b (mm)	δ (mm)	d (m)
1.37	1.13	1	100	5	1

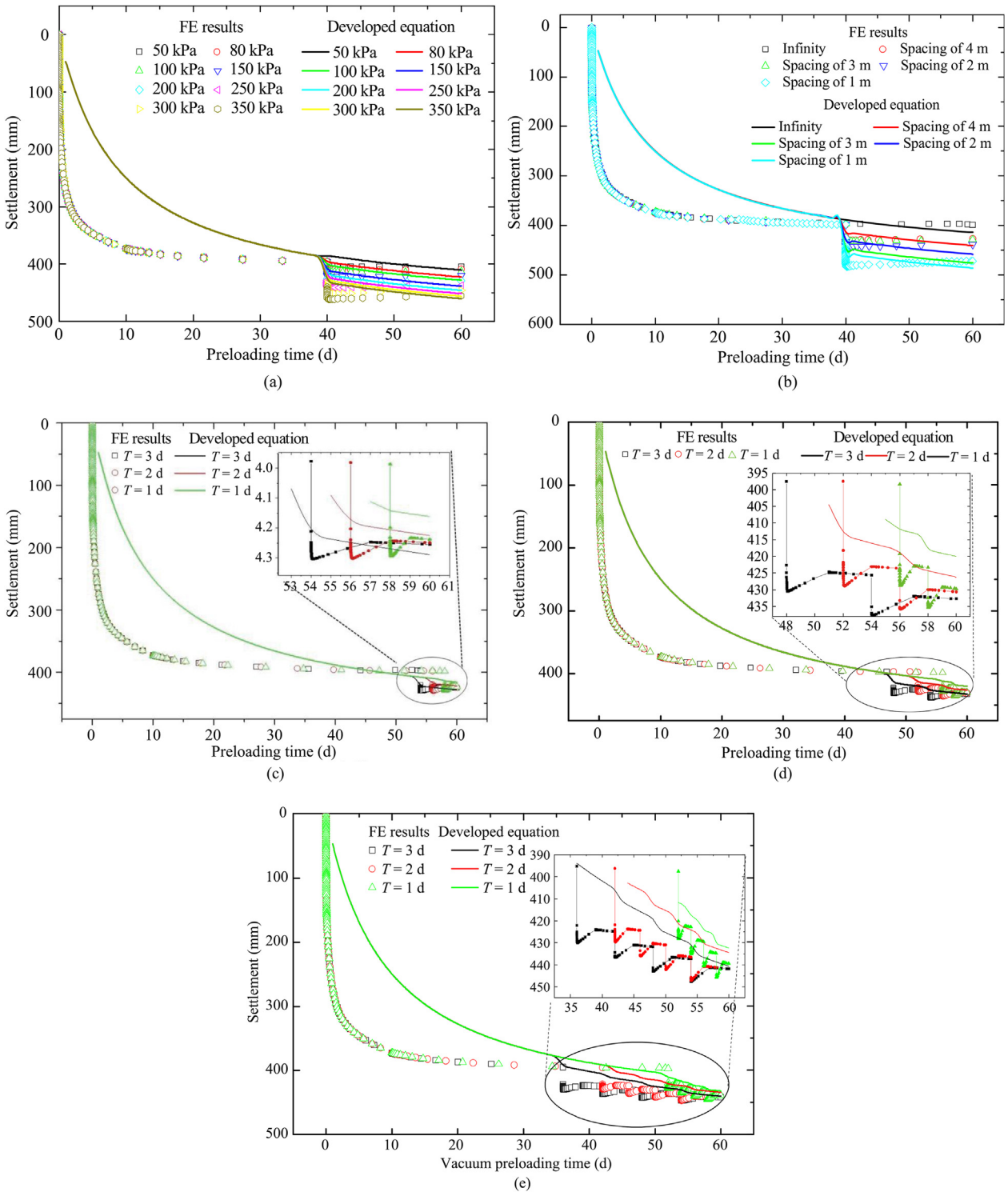

Fig. 18. Comparison between the closed-form equation and the 3D FE analyses: (a) Effect of the injection pressure; (b) Effect of the injection spacing; and (c–e) Effect of injection cycle, i.e. (c) $N = 1$, (d) $N = 2$, and (e) $N = 4$.

Table 4
Parameters of the developed equation.

α	β	d_p	d_s	d_{in}
0.0062	0.0005	−0.07	0.025	0.08

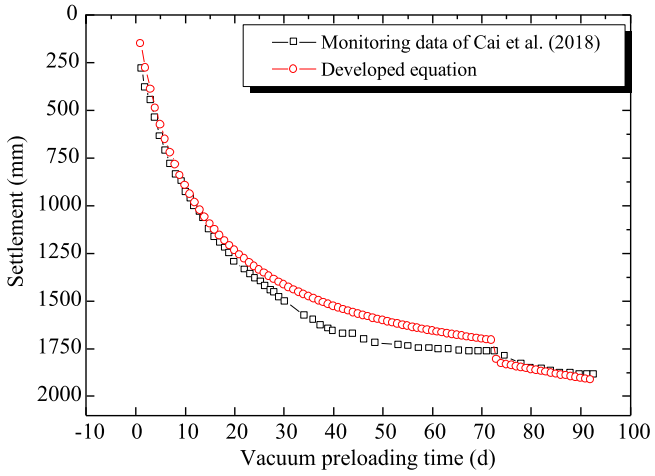

Fig. 19. Comparison of the closed-form solution to the field test data.

utilized to calculate the consolidation settlement due to air-boosted vacuum preloading.

Following the above steps, the closed-form expression was used to calculate the numerical cases listed for the three-dimensional (3D) FE modeling. Although the closed-form expression was deduced based on the 3D FE parametric analyses, not all parameters were obtained from the FE analyses. For example, the parameters α and β were theoretically derived, i.e. decoupled from the 3D FE analyses. Therefore, the comparison between the proposed closed-form expression and the 3D FE analyses is necessary to assess the accuracy of the closed-form expression. Fig. 18 shows the comparative results between the 3D FE analyses and the closed-form equation. For the various injection pressures, injection spacings and injection cycles considered, the predicted ground settlement using the closed-form expression was reasonably comparable to the 3D FE modeling results. In the following section, the proposed closed-form solution is applied to a case reported in the literature to further assess its validity.

4.2. Application of the proposed closed-form equation

The applicability of the proposed closed-form equation is evaluated against the field test results reported by Cai et al. (2018). The field tests were carried out in Wenzhou, China, where the vacuum preloading lasted for 92 d, including 72 d of vacuum preloading and 20 d of air-boosted vacuum preloading. The average degree of consolidation was 74% for 72 d of vacuum preloading. At the end of the vacuum preloading in conjunction with air injection, an average degree of consolidation of 80% was required. This design information is useful for the calculation of α. Moreover, the stratigraphic details were employed to calculate β. The depth of the vacuum preloading was 20 m, and the top-down soil profile consisted of 1.55 m thick silt, 6.8 m muddy-silt clay, 4.9 m silt clay, 5 m silt clay and 4.85 m silt. The corresponding void ratios before vacuum preloading were 1.645, 1.5, 1.205, 1.555 and 1.655, respectively, while the void ratios after vacuum preloading were 1.21, 1.16, 1.01, 1.17 and 1.24, respectively.

The air injection pressure was $p = 20$ kPa, the injection spacing was $s = 1.6$ m, the total number of air injection cycles was $N = 20$ and the air injection time per cycle was $T = 2$ h until the end of the preloading. Given the above information, using Eqs. (17), (18) and (4), d_p, d_s and d_{in} were determined. The parameters required for Eq. (9) are summarized in Table 4. The results calculated by the closed-form equation are compared with the monitoring data (Cai et al., 2018) in Fig. 19. Overall, the results were in excellent agreement, and the largest discrepancy was less than 2% during vacuum preloading alone and approximately 1.5% during air-boosted vacuum preloading.

5. Conclusions

This study presents field tests and numerical modeling of ground surface settlement and lateral displacement of dredged sediments treated with air-boosted vacuum preloading. In addition, a simple and practical closed-form formula is proposed to predict the consolidation settlement, considering the influencing factors of air injection pressure, injection spacing, and characteristics of cyclic injection. The main conclusions are drawn as follows:

(1) Compared with conventional vacuum preloading, air-boosted vacuum preloading enhanced the consolidation rate of soft ground, with ground settlement and soil undrained shear strength increasing by 11.7% and 5.7%–21.8%, respectively.
(2) An increase in the injection pressure led to increases in the ground settlement and soil lateral displacement. For air injection pressures ranging from 50 kPa to 350 kPa, the ground settlement increased by 1.5%–12.3% compared to that under vacuum loading alone. The corresponding lateral displacement was approximately 23%–33% of the ground settlement. In general, the lateral displacement was greater at shallower depths, which could lead to potential cracks near the ground surface.
(3) A decrease in the injection spacing increased the ground settlement and the lateral displacement. A 1-m decrease in the injection spacing increased the ground settlement and lateral displacement by 18.3% and 17.7%, respectively. It could be beneficial to impose cyclic air injections rather than continuous air injection and a longer duration of cyclic injection to enhance the consolidation.

A simple and practical closed-form expression was developed to estimate ground settlement by air-boosted vacuum preloading, which included the effects of the injection pressure, the injection spacing, the number of injection cycles, and the injection period. This equation was validated against the 3D FE analyses and a full-scale case reported in the literature.

Declaration of competing interest

The authors declare that they have no known competing financial interests or personal relationships that could have appeared to influence the work reported in this paper.

Acknowledgments

The authors acknowledge the National Key Research and Development Program of China (Grant No. 2017YFC0805402), the Tianjin Construction Commission Science and Technology Project (financial support No. 2017E6-0015), and the China Scholarship

Council (CSC) (Grant No. 201906250153) for their Grant of the study in this paper.

References

Anda, R., Fu, H., Wang, J., Lei, H., Hu, X., Ye, Q., Cai, Y., Xie, Z., 2020. Effects of pressurizing timing on air booster vacuum consolidation of dredged slurry. Geotext. Geomembr. 48 (4), 491–503.

Cai, Y., Xie, Z., Wang, J., Wang, P., Geng, X., 2018. New approach of vacuum preloading with booster PVDs to improve deep marine clay strata. Can. Geotech. J. 55 (10), 1359–1371.

Feng, S., Lei, H., Ding, X., Zheng, G., Jin, Y., 2021. Shallow ground treatment by a combined air booster and straight-line vacuum preloading method: a case study. Geomech. Eng. 24 (2), 129–141.

Gangaputhiran, S., Robinson, R.G., Karpurapu, R., 2016. Properties of soil after surcharge or vacuum preloading. Proc. Inst. Civil Eng. Geotech. Eng. 169 (3), 217–230.

GB/T 50123–2019, 2019. Standard for Geotechnical Testing Method. China Planning Press, Beijing, China in Chinese.

Goh, A.T., Zhang, Y., Zhang, R., Zhang, W., Xiao, Y., 2017. Evaluating stability of underground entry-type excavations using multivariate adaptive regression splines and logistic regression. Tunn. Undergr. Space Technol. 70, 148–154.

Gouw, T.L., 2020. Case histories on the application of vacuum preloading and geosynthetic-reinforced soil structures in Indonesia. Indian Geotech. J. 50 (2), 213–237.

Griffin, H., O'Kelly, B.C., 2014. Ground improvement by vacuum consolidation – a review. Geotext. Geomembranes 167 (4), 274–290.

Indraratna, B., Kan, M., Potts, D., Rujikiatkamjorn, C., Sloan, S., 2016. Analytical solution and numerical simulation of vacuum consolidation by vertical drains beneath circular embankments. Comput. Geotech. 80, 83–96.

Indraratna, B., Rujikiatkamjorn, C., Baral, P., Ameratunga, J., 2019. Performance of marine clay stabilised with vacuum pressure: based on Queensland experience. J. Rock Mech. Geotech. Eng. 11 (3), 598–611.

JTS 147–2–2009, 2009. Technical Specification for Vacuum Preloading Technique to Improve Soft Soils. China Communications Press, Beijing, China in Chinese.

Ke, S., Wang, P., Hu, X., Geng, X., Hai, J., Jin, J., Chen, Z., 2020. Effect of the pressurized duration on improving dredged slurry with air booster vacuum preloading. Mar. Geores. Geotechnol. 38 (8), 970–979.

Kjellman, W., 1952. Consolidation of clayey soils by atmospheric pressure. In: Proceeding of the Conference on Soil Stabilization. Massachusetts Institute of Technology, Boston, USA, pp. 258–263.

Lei, H., Feng, S., Wang, L., Jin, Y., 2019. Field instrumentation and settlement prediction of ground treated with straight-line vacuum preloading. Geomech. Eng. 19 (5), 447–462.

Lei, H., Lu, H., Liu, J., Zheng, G., 2017. Experimental study of the clogging of dredger fills under vacuum preloading. Int. J. GeoMech. 17 (12). https://doi.org/10.1061/(ASCE)GM.1943-5622.0001028.

Liu, J., Lei, H., Zheng, G., Zhou, H., Zhang, X., 2017a. Laboratory model study of newly deposited dredger fills using improved multiple-vacuum preloading technique. J. Rock Mech. Geotech. Eng. 9 (5), 924–935.

Liu, Y., Qi, L., Li, S., Guo, H., 2017b. 3D Finite element analysis of vacuum preloading considering inconstant well resistance and smearing effects. Rock Soil Mech. 38 (5), 1517–1523 (in Chinese).

Mesri, G., Khan, A., 2012. Ground improvement using vacuum loading together with vertical drains. Mar. Georesour. Geotechnol. 138 (6), 680–689.

Nguyen, B., Yun, D., Kim, Y., 2018. An equivalent plane strain model of PVD-improved soft deposit. Comput. Geotech. 103, 32–42.

Saleh, S., Yunus, N., Ahmad, K., Said, K., 2021. Numerical simulation with hardening soil model parameters of marine clay obtained from conventional tests. SN Appl. Sci. 3 (2), 156.

Schanz, T., Vermeer, P.A., Bonnier, P.G., 1999. The hardening soil model: formulation and verification. In: Beyond 2000 in Computational Geotechnics – 10 Years of PLAXIS. A.A. Balkema, Rotterdam, Netherlands, pp. 281–296.

Shen, Y., Wang, H., Tian, Y., Feng, R., Liu, J., Wu, L., 2015. A new approach to improve soft ground in a railway station applying air-booster vacuum preloading. Geotech. Test J. 38 (4), 373–386.

Shibata, T., Murakami, A., Fujii, M., 2014. Prediction of embankment behavior of regulating reservoir with foundation improved by vacuum consolidation method. Soils Found. 54 (5), 938–954.

Uy, E.E.S., Dungca, J., 2018. A comparative settlement prediction of limestone blended materials using Asaoka and hyperbolic method. Int. J. GEOMATE 14 (43), 63–69.

Voottipruex, P., Bergado, D.T., Wongprasan, W., 2013. Simulations of PVD improved reconstituted specimens with surcharge, vacuum and heat preloading using axisymmetric and equivalent vertical flow conditions. Geotech. Eng. 44 (4), 61–68.

Wang, J., Cai, Y., Ma, J., Chu, J., Fu, H., Wang, P., Jin, Y., 2016. Improved vacuum preloading method for consolidation of dredged clay-slurry fill. J. Geotech. Geoenviron. Eng. 142 (11). https://doi.org/10.1061/(ASCE)GT.1943-5606.0001516.

Xie, L., Niu, Y., Liu, F., Liu, S., 2009. Numerical analysis of vacuum drainage with air injection. Chin. J. Undergr. Space Eng. 5 (S2), 1590–1593 (in Chinese).

Zheng, G., Liu, J., Lei, H., Rahman, M.S., Tan, Z., 2017. Improvement of very soft ground by a high-efficiency vacuum preloading method: a case study. Mar. Geores. Geotechnol. 35 (5), 631–642.

Shuangxi Feng is presently working as a post-doctor, assistant research fellow, at Tianjin University, China. He obtained his PhD degree from the same university. He has vast practical experience in soft soil treatment, soft soil engineering property and constitutive relation of soil. He has participated in the national major R&D project, the National Natural Science Foundation project, and 4 provincial and ministerial and engineering cooperation projects. Dr. Feng has published 21 academic papers, including 8 papers indexed by SCI and 5 papers indexed by EI. He also obtained 8 patents, including 4 invention patents and 4 utility model patents.